Materials Transactions, Vol. 67, No. 9 (2026) pp. 1451 to 1461

OVERVIEW

Material Degradation of Heat-Resistant Steels during Long-Term Creep Exposure

Kota Sawada*

National Institute for Materials Science, Tsukuba 305-0047, Japan

Creep strength and material degradation of heat-resistant steel were discussed, focusing on microstructural changes during long-term creep exposure. The materials and creep rupture data were obtained from Creep Data Sheet Project by National Institute for Materials Science. For determining the allowable stress, the 100,000 h creep rupture strength should be evaluated based on creep rupture data. The selection of TTP and dividing the creep rupture data set are important to evaluate long-term creep strength when creep strength degradation occurs in the long term. In order to establish the allowable stress, minimum creep strength must also be evaluated. The minimum creep strength depends on the standard error of estimate (SEE) for creep rupture data. If the heat-to-heat variation of creep strength is large even for the same material specification, the value of SEE is estimated to be large. Therefore, it is important to clarify the reason for the heat-to-heat variation of creep strength in terms of microstructural changes and chemical compositions. Microstructural degradations were reported for carbon steels, low alloy steels, 9–12%Cr ferritic steels and austenitic heat-resistant steels, focusing on precipitates and dislocation structures. The reason for the heat-to-heat variation of creep rupture strength was discussed in term of the difference of solute atoms, segregation and grain size.
[doi:10.2320/matertrans.MT-M2026047]

(Received April 24, 2026; Accepted May 30, 2026; Published August 25, 2026)

Keywords: *heat-resistant steels, long-term creep, microstructural changes, heat-to-heat variation*

1. Introduction

With renewable energy increasingly being introduced worldwide to reduce CO_2 emissions from the energy sector, thermal power plants are needed to cover the fluctuations in output from renewable energy. Under such circumstances, thermal power plants are operated not as base load but under partial load, leading to cyclic loading on the components of the plants [1]. Accordingly, not only the creep properties but also the creep-fatigue properties should be evaluated to improve the reliability of such components [2, 3]. On the other hand, the fuel used in coal-fired thermal power plants will be switched from coal to hydrogen and/or ammonia, thus reducing CO_2 emissions [4]. Therefore, it is still important to evaluate the creep strength of heat-resistant steels to ensure the safe operation of thermal power plants.

In the nuclear power sector, next-generation nuclear reactors such as fast reactors and high-temperature gas-cooled reactors are actively being developed to meet the increasing global demand for power [5, 6]. The design life of these reactors is several decades [7], and so the ultra-long-term creep strength of heat-resistant steels and alloys should be evaluated to establish the allowable stress. For example, 60-year creep rupture strength was estimated for ASME Grade 91 steels to establish the allowable stress for the ASME Boiler and Pressure Vessel code [8].

When introducing new heat-resistant steels and alloys, the allowable stress should be established based on long-term creep strength evaluations because the wall thickness of boiler tubes and pipes is designed based on the allowable stress. Recently, ASME Grade 93 [9] and HR6W [10] developed in Japan were standardized based on long-term creep data and the allowable stress for thermal power plants was established. For existing heat-resistant steels, allowable stress and chemical compositions were reviewed based on long-term creep data. For creep strength enhanced ferritic steels, Grade 91, 92 and 122, the allowable stresses were reduced [11, 12] because it was clear that the 100,000 h creep rupture strength was an overestimation due to long-term degradation of creep strength [13, 14].

For establishing the allowable stress for thermal power plants, the 100,000 h creep rupture strength is determined based on regression analysis of creep rupture data and time-temperature parameters (TTP) such as the Larson–Miller parameter [15]. TTP suitable for material properties should be selected to accurately estimate the 100,000 h creep rupture strength. The minimum value of creep rupture strength is also needed to establish the allowable stress [16]. This minimum value depends on the statistical dispersion of creep rupture strength [17]. However, not experimental error but metallurgical factors can cause dispersion in some cases even for the same material specification. It is predicted that the chemical compositions and heat treatment conditions of the material specification will be reviewed when metallurgical factors strongly affect the dispersion of creep rupture strength. Therefore, when revising chemical compositions and heat treatment conditions it is important to clarify the metallurgical factors.

The National Institute for Materials Science (NIMS) started the Creep Data Sheet project in 1966 to obtain the 100,000 h creep rupture strength of heat-resistant steels and alloys [18]. In this project, creep testing of multi-heat for the same material specification was performed. The degradation of materials and heat-to-heat variation of creep strength have been investigated for heat-resistant steels and alloys. Furthermore, the effects of chemical composition and microstructural factors on the degradation of materials and heat-to-heat variation of creep strength have been examined. In the present overview, creep strength evaluation, allowable stress, material degradation during long-term creep and heat-to-heat variation of creep strength are discussed based on long-term creep data obtained from NIMS Creep Data Sheets.

*Corresponding author, E-mail: sawada.kota@nims.go.jp

2. Method of Evaluating Creep Strength and Allowable Stress

For determining the allowable stress, the 100,000 h creep rupture strength is evaluated based on creep rupture data. Regression analysis of the creep rupture data is performed using a regression equation of logarithmic stress with TTP to estimate the 100,000 h creep rupture strength. For example, Larson–Miller (LM) [15], Orr–Sherby–Dorn (OSD) [19] and Manson–Haferd (MH) [20] parameters are used as typical TTP:

$$\text{LM} \quad TTP = (T + 273.15)(C + \log t_R) \tag{1}$$

$$\text{OSD} \quad TTP = \log t_R - Q/[2.3R(T + 273.15)] \tag{2}$$

$$\text{MH} \quad TTP = (\log t_R - \log t_a)/(T + 273.15 - T_a) \tag{3}$$

where t_R = time to rupture (h), T = temperature (°C), C, Q, t_a, and T_a = optimized constants, and R = the gas constant.

The master creep rupture curve for the fitting is expressed as follows:

$$TTP = b_0 + b_1 \log S + b_2(\log S)^2 + \ldots + b_k(\log S)^k \tag{4}$$

$$TTP = b + b_0 S + b_1 \log S + b_2(\log S)^2 + \ldots + b_k(\log S)^k \tag{5}$$

where S = stress (MPa), $b, b_0, b_1, b_2, b_3, \ldots, b_k$ = regression coefficients estimated by the least squares method, and k = degree of regression equation.

Normally, all the creep rupture data are used for the regression analysis. However, in some cases, the fitting curve (dashed line) overestimates the long-term creep strength when the creep strength abruptly degrades in the long term as shown in Fig. 1. It is recommended that creep rupture data of less than 500 h should not be used for the regression analysis in the ASME code [16]. Region-splitting analysis was proposed [14] for the regression analysis in the event of occurrence of creep strength degradation in the long term. In this method, creep rupture data are divided into two regions by the half value of 0.2% proof stress at each temperature, which corresponds to the proportional limit [21]. Plastic deformation can easily occur during creep exposure when stress exceeds the proportional limit. On the other hand, creep deformation can occur in relatively weak areas such as grain boundaries under low stress that is less than the half value of 0.2% proof stress. For modified 9Cr-1Mo steels, tempered martensite homogeneously recovered during creep exposure under high stress. However, preferential recovery occurred around prior austenite grain boundaries during creep exposure under low stress in modified 9Cr-1Mo steels [13]. Figure 2 shows the result of region-splitting analysis for creep rupture data of ASME Grade 91 steels (modified 9Cr-1Mo steel). The LM parameter was used for the two regions [22]. Creep strength can be accurately evaluated in the long term even if creep strength degradation occurs in the long term.

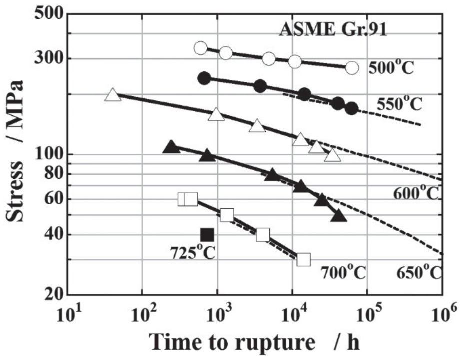

Fig. 1 Creep rupture strength of ASME Grade 91 steel.

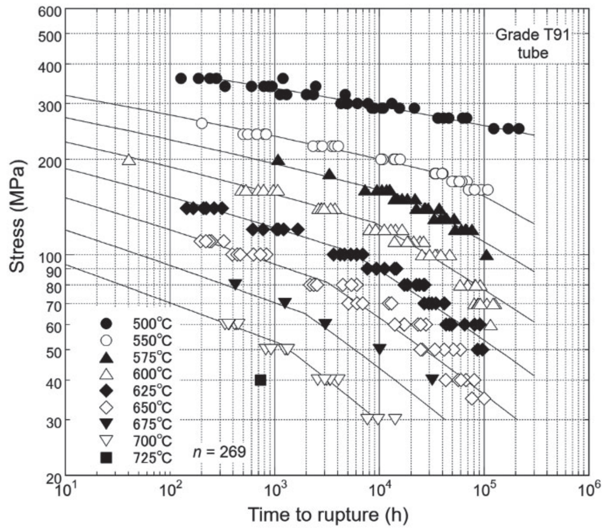

Fig. 2 Result of region splitting analysis for creep rupture data of Grade T91.

Multiregion analysis was also proposed for evaluating creep strength [23]. In this method, creep rupture data are divided into multiple regions based on the activation energy for creep rupture time. For example, the activation energy decreases in the long term for ASME Grade 91 steel [24]. Creep strength can be accurately estimated in the long term by multiregion analysis based on the change of activation energy for creep rupture time. Region-splitting analysis is useful when there is not enough creep rupture data for the very long-term region. On the other hand, multiregion analysis can accurately evaluate long-term creep strength when the activation energy can be estimated using enough long-term creep rupture data.

Consequently, both the selection of TTP and dividing the creep rupture data set are important to evaluate long-term creep strength when creep strength degradation occurs in the long term. Therefore, it is important to identify the metallurgical factors causing creep strength degradation in the long term.

The analysis method mentioned above evaluates average creep strength. In order to establish the allowable stress, minimum creep strength must also be evaluated [16]. For example, the minimum creep strength [17] is expressed as follows from eq. (1) and eq. (4) in case of the LM parameter:

$$\log t_R = (T + 273.15)^{-1}[b_0 + b_1 \log S + b_2(\log S)^2 + \ldots + b_k(\log S)^k] - C - 1.65\text{SEE} \tag{6}$$

where SEE = the standard error of estimate. If the heat-to-heat variation of creep strength is large even for the same material specification, the value of SEE is estimated to be large. This means the minimum creep strength is very low. To improve the allowable stress, not only average creep strength but also minimum creep strength should be increased, indicating that the heat-to-heat variation of creep strength should be small. Therefore, it is important to clarify the reason for the heat-to-heat variation of creep strength in terms of microstructural changes and chemical compositions. Equation (6) is also used to estimate the life of operating plants. The coefficient of SEE in eq. (6) depends on the confidence interval. The heat-to-heat variation of creep strength can also affect the estimation of life of operating plants. For conventional heat-resistant steels, product form, chemical composition and heat treatment condition can affect the heat-to-heat variation for the same material specification. Recently, creep strength was evaluated for heat-resistant materials by additive manufacturing [25, 26]. In this case, not only the factors mentioned above but also build direction may be a reason for the heat-to-heat variation of creep strength [25].

3. Material Degradation during Long-Term Creep Exposure

3.1 Carbon steels and low alloy steels

Normally, carbon steels and low alloy steels consist of ferrite and pearlite. Figure 3 shows SEM images of creep ruptured specimens of 0.2C silicon-killed steel, JIS STB 410 [27]. The spheroidization of pearlite structure occurred after creep rupture and was remarkable at higher temperatures in the long term. Stress promotes spheroidization during creep exposure [28]. However, no remarkable drop in creep rupture strength was confirmed in the long term for carbon steels [27]. It was reported that a large drop in creep strength occurred in the long term for carbon steel with high nitrogen [29]. In this case, the solid solution nitrogen contributed to the creep rupture strength in the short term. However, the creep rupture strength degraded in the long term because the amount of solid solution nitrogen decreased during creep exposure due to precipitation of nitride [29]. In addition to the spheroidization of pearlite, graphitization can occur during long-term creep exposure in carbon steels. It was reported that graphite was formed after creep exposure for 232,983.5 h at 400°C in 0.3%C steel [30] although Japanese Industrial Standards (JIS) [31] and Japan Petroleum Institute (JPI) Standard [32] note the occurrence of graphitization above 425°C. Figure 4 shows SEM micrograph of a creep ruptured specimen for 0.3%C steel. Elongated graphite was observed after creep rupture even at 400°C [30]. Spherical graphite can also be formed after creep rupture [30]. Elongated graphite tends to form during creep exposure under higher stresses [30]. Graphite may serve as the origin of fracture of components after long-term operation in power

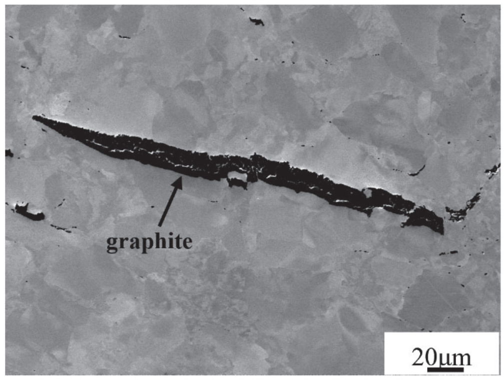

Fig. 4 Graphite observed in creep ruptured specimen of 0.3C steel. 400°C, tr = 232,983.5 h.

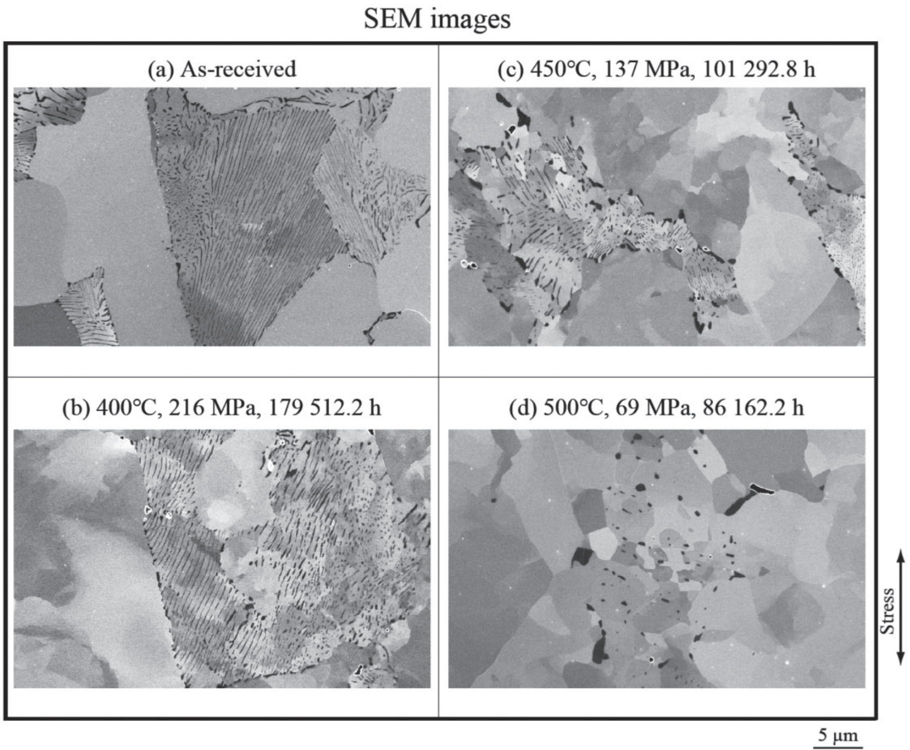

Fig. 3 SEM images of creep ruptured specimens of 0.2C silicon-killed steel.

plants [33]. Therefore, it is important to identify the time and temperature of occurrence of graphitization. The time-temperature-precipitation diagrams of graphitization were also reported for 0.2C, 0.3C and 0.5Mo steels [34].

For low alloy steels, ferrite-pearlite, bainite and martensite structures can be used depending on heat treatment. The creep rupture strength of the martensite structure is compared with that of the ferrite-pearlite structure for 2.25Cr-1Mo steel in Fig. 5 [35]. The creep strength of martensite is far superior to that of ferrite-pearlite in the short term while no difference in creep rupture strength was observed between martensite and ferrite-pearlite structures in the long term. It was confirmed that the martensite and pearlite structures disappeared after long-term creep exposure (Fig. 6), meaning that the ferrite structure remained for both steels [35]. That is why the creep strength of the martensite structure was almost the same as that of the ferrite-pearlite structure in the long term. Therefore, microstructural changes during creep exposure should be retarded to improve long-term creep strength. It was reported that in 0.5Cr-0.5Mo steels, the long-term creep strength of the ferrite-pearlite structure was higher than those of bainite, tempered martensite and martensite structures [36]. In addition to recovery of pearlite and martensite structures during creep exposure, a precipitation free zone (PFZ) forms around grain boundaries during creep exposure in low alloy steels [37]. The PFZ spreads with increasing creep time [37]. Creep deformation can become concentrated in the PFZ because precipitation strengthening is reduced in the PFZ. It is predicted that creep voids can form on grain boundaries due to the concentration of creep deformation in the PFZ. Therefore, not only the recovery of pearlite and martensite structures during creep exposure but also the formation of PFZ contribute to the creep strength degradation of low alloy steels.

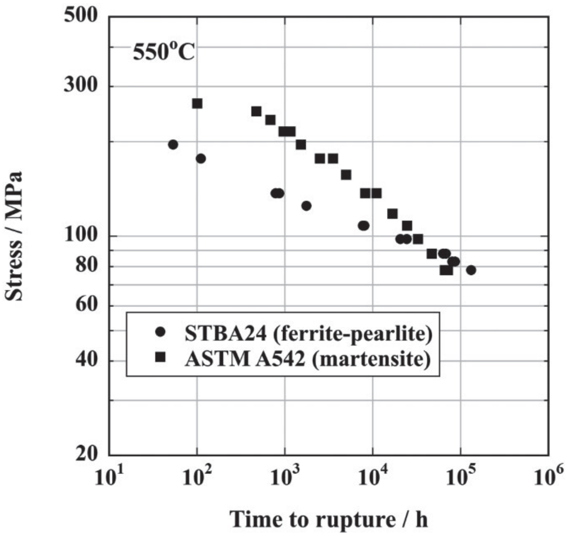

Fig. 5 Creep rupture strength of 2.25Cr-1Mo steels at 550°C.

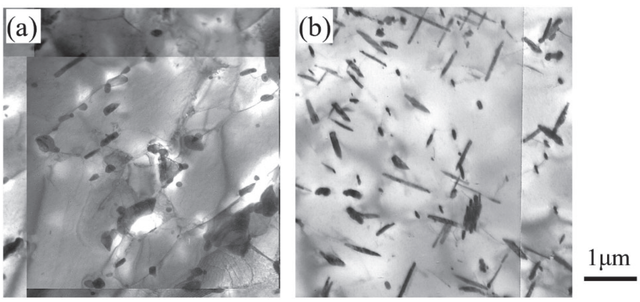

Fig. 6 TEM images of creep ruptured specimens of 2.25Cr-1Mo steel. (a) STBA24 (initial: ferrite-pearlite): 550°C, tr = 46,816.8 h. (b) ASTM A542 (initial: martensite): 550°C, tr = 85,906.2 h.

3.2 9–12%Cr ferritic steels

In this section, 9–12%Cr ferritic steels with tempered martensitic structure are discussed. 9–12%Cr ferritic steels are widely used for ultra-supercritical power plants because of their good creep strength [38]. For example, 9–12%Cr ferritic steels such as ASME Grade 91 [39], Grade 92 [39] and Grade 122 [39] steels have the nominal composition of 9Cr-1Mo-V-Nb-N, 9Cr-0.5Mo-1.8W-V-Nb-N and 11Cr-2W-0.4Mo-1Cu-Nb-V, respectively. 9–12%Cr ferritic steels are strengthened by a tempered martensitic structure, $M_{23}C_6$ (M: Cr, Mo, W) carbide and MX (M: V, Nb, X: C, N) carbonitride as shown in Fig. 7 [40]. Mo and W can also contribute to solid solution strengthening [41]. The martensitic structure of creep interrupted specimens is shown in Fig. 8 together with hardness value [42]. The martensitic structure recovered during creep exposure and this recovery caused a decrease in hardness during creep exposure. The martensitic structure disappeared and changed to equiaxed subgrains after creep rupture as shown in Fig. 8(d). For

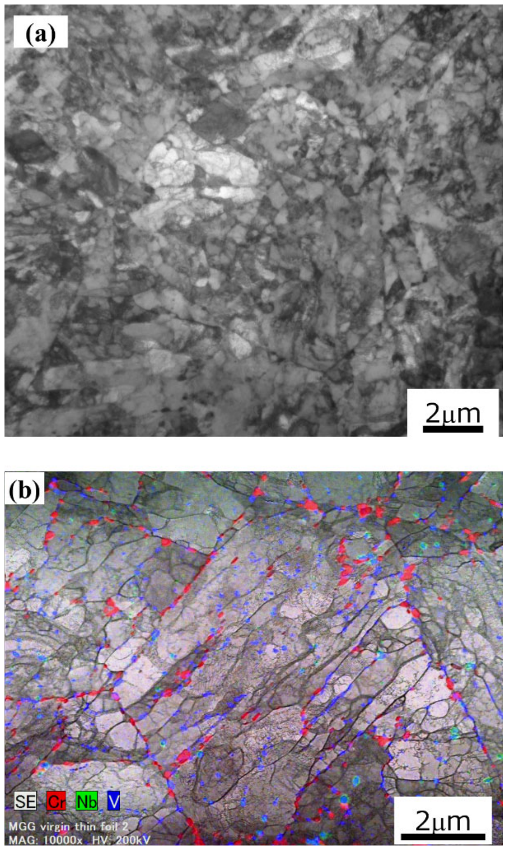

Fig. 7 (a) TEM micrograph of as received material of ASME Grade 91 steel, (b) Result of elemental map by STEM-EDS for as received material of ASME Gr.91 steel. Red particle: $M_{23}C_6$, Blue particle: V-rich MX, Green particle: Nb-rich MX. (online color)

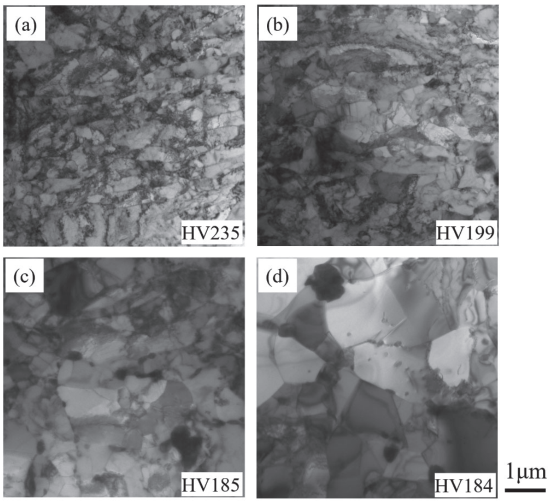

Fig. 8 TEM micrographs of as received and crept materials of ASME Grade 91 steel. (a) Before creep, (b) 600°C/50,000 h, (c) 600°C/70,000 h, (d) 600°C/80736.8 h.

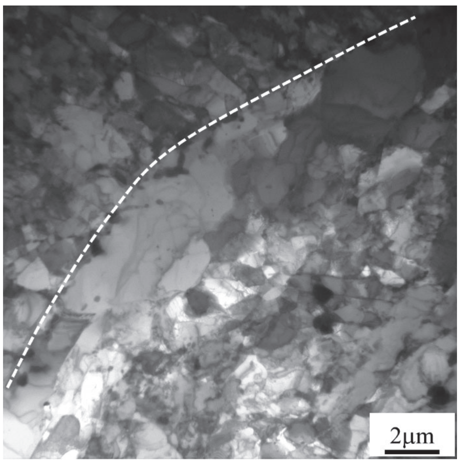

Fig. 9 Preferential recovery around prior austenite grain boundary after creep rupture in Grade 91 steel. 600°C, 110 MPa, tr = 24.189.1 h. Dashed line: prior austenite grain boundary.

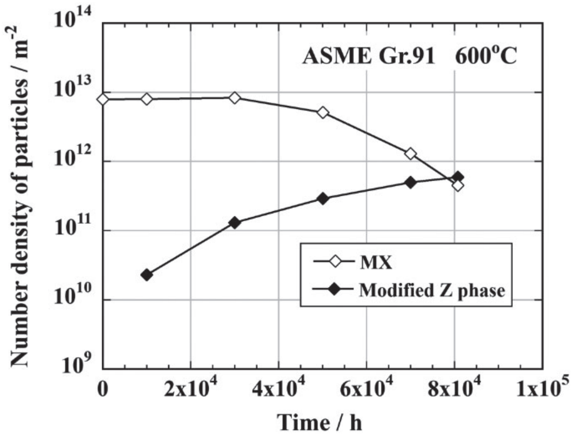

Fig. 10 Formation of modified Z phase during creep exposure together with disappearance of MX.

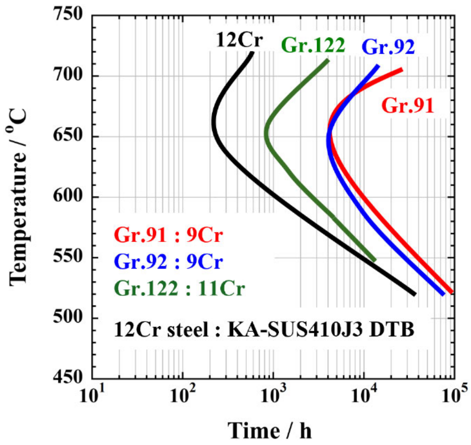

Fig. 11 Effect of Cr content on time-temperature-precipitation diagram of modified Z phase. (online color)

ASME Grade 91 steel, the creep strength abruptly degrades in the long term as shown in Fig. 2. The martensitic structure homogenously recovered during creep exposure under high stress while preferential recovery of martensite occurred around prior austenite grain boundaries under low stress as shown in Fig. 9. Therefore, the preferential recovery can contribute to the creep strength degradation in the long term [13], as was also reported for Grade 92 and Grade 122 steels [43]. The martensitic structure can statically recover during aging [23]. It was reported that creep strength degradation can occur when the static recovery of the martensitic structure is remarkable during aging [23].

Coarsening of $M_{23}C_6$ and MX precipitates occurs during long-term creep exposure, causing a decrease in precipitation strengthening. This process is basically explained by Ostwald ripening [44, 45]. It was reported that the addition of B can retard the coarsening of $M_{23}C_6$ during creep exposure in 9%Cr steel [46]. Creep stress and/or strain promotes the coarsening of precipitates during creep exposure [47]. In addition to the coarsening of precipitates, the formation of a harmful phase can occur during creep exposure and decrease long-term creep strength. Modified Z phase [Cr(V, Nb)N] is harmful to creep strength [48] because its formation consumes fine MX precipitates during long-term creep exposure as shown in Fig. 10. It was reported in 12%Cr steels that Cr in the matrix diffuses to MX precipitates during creep exposure and MX precipitates gradually transform to modified Z phase [49]. Figure 11 shows the time-temperature-precipitation diagram of modified Z phase in 9–12%Cr steels [50]. An increase in Cr content promoted the formation of modified Z phase during creep exposure as shown in Fig. 11. An increase in Ni content can also promote the formation of modified Z phase during creep exposure [51, 52]. Accordingly, the Cr and Ni contents should be reduced to avoid the formation of modified Z phase during creep exposure in 9–12%Cr steels. Danielsen *et al.* reported the effect of elements on the driving force of the formation of modified Z phase, using Thermo-calc [53]. The addition of N can increase the driving force. Laves phase such as Fe_2Mo and Fe_2W is formed during creep exposure [54, 55]. This phase can provide nucleation sites for creep voids because the size of the Laves phase is larger than those of $M_{23}C_6$ and MX [56]. The Laves phase can contribute to precipitation strengthening, but the effect of Laves phase formation on creep strength is unclear because the formation consumes

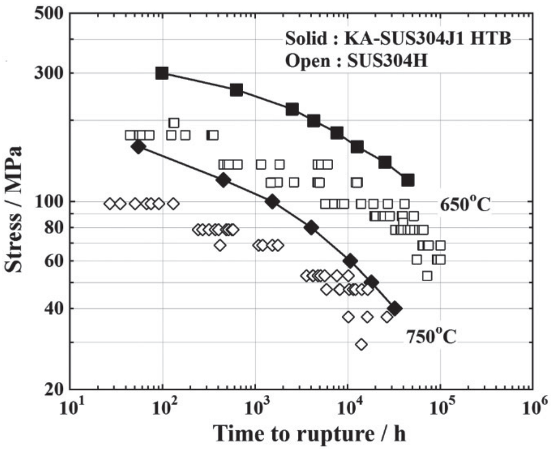

Fig. 12 Creep rupture strengths of KA-SUS304J1HTB and SUS304H.

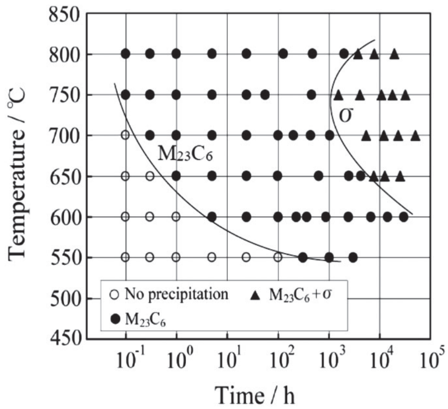

Fig. 13 Time-temperature-precipitation diagram of $M_{23}C_6$ and σ phase in KA-SUS304J1HTB.

solute Mo and W which contribute to solid solution strengthening [41].

3.3 Austenitic heat-resistant steels

Figure 12 shows the creep rupture strength of SUS304HTB (18Cr-8Ni) [57] and KA-SUS304J1HTB (18Cr-9Ni-3Cu-Nb-N) [58]. The creep strength is higher in KA-SUS304J1HTB than in SUS304HTB. The creep strength of KA-SUS304J1HTB was improved by the addition of Cu and Nb to SUS304HTB [59]. However, the creep strength of both steels degrades in the long term. The difference in creep strength between the two steels becomes small in the long term because the creep strength degradation is remarkable for KA-SUS304J1HTB as compared with SUS304HTB. Normally, no precipitates except for inclusions are observed before creep exposure for both steels because solution heat treatment is performed. $M_{23}C_6$ and sigma phase are formed during creep exposure for both steels.

For KA-SUS304J1HTB, the time-temperature-precipitation diagram of $M_{23}C_6$ and sigma phase during aging are shown in Fig. 13. The sigma phase is formed after $M_{23}C_6$ formation during aging. Figure 14 shows SEM micrographs of the grip portion of creep ruptured samples for KA-SUS304J1HTB. The precipitates shown in black are $M_{23}C_6$ particles. Fine $M_{23}C_6$ particles are formed on grain boundaries after short-term aging. These particles contribute

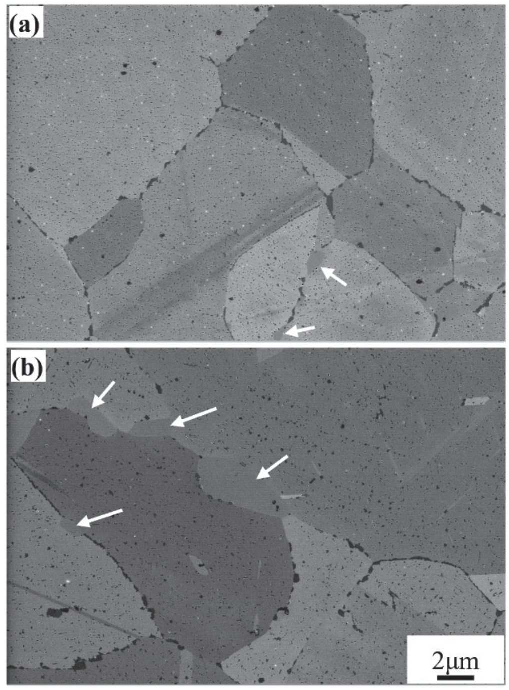

Fig. 14 SEM micrographs of grip portion of creep ruptured specimens of KA-SUS304J1HTB. (a) 650°C, 7636.9 h. (b) 650°C, 44602.7 h. Black particles: $M_{23}C_6$. Arrows indicate σ phase.

to grain boundary strengthening [60]. On the other hand, coarse sigma phase is formed on grain boundaries and consumes $M_{23}C_6$ particles after long-term aging as shown in Fig. 14. Therefore, the formation of sigma phase can cause creep strength degradation in the long term. Fine NbX particles and Cu phase are also formed after short-term creep in KA-SUS304J1HTB [61] in contrast to SUS304HTB. The NbX particles change to modified Z phase after long-term creep [61]. The modified Z phase can contribute to precipitation strengthening because the size of the modified Z phase is small in contrast to 9–12%Cr steels. Cu phase is coherently formed in the matrix after short-term creep and contributes to precipitation strengthening [62]. However, the coherency disappears due to coarsening after long-term creep, contributing to creep strength degradation [62]. The creep fracture mode changes depending on stress and temperature for both steels [63, 64]. Transgranular or wedge type fractures can occur under a high stress condition and cracking at the sigma phase/matrix interface is seen under a low stress condition [63, 64]. Figure 15 shows a TEM micrograph after long-term creep exposure for KA-SUS304J1HTB. It is clearly seen that a PFZ is formed around the sigma phase on grain boundaries [65]. It is predicted that creep deformation is concentrated on the PFZ and creep voids can form at the sigma phase/matrix interface. Schematic illustrations of microstructural changes after creep exposure are compared between SUS304HTB and KA-SUS304J1HTB as shown in Fig. 16. $M_{23}C_6$ precipitates are observed in the grain interior for SUS304HTB while fine Cu phase, NbX and modified Z phase are distributed in the grain interior for KA-SUS304J1HTB after short-term creep exposure. Therefore, the precipitation strengthening in the grain interior is higher in KA-SUS304J1HTB than in SUS304HTB. Sigma phases are formed on grain boundaries

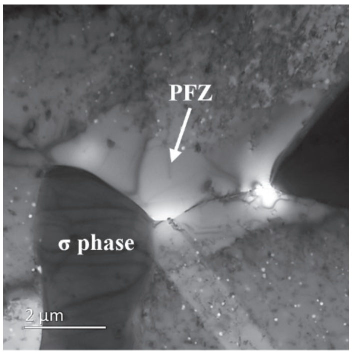

Fig. 15 PFZ around σ phase on grain boundary in creep ruptured specimen of KA-SUS304J1HTB. 700°C, 60 MPa, tr = 50214.3 h.

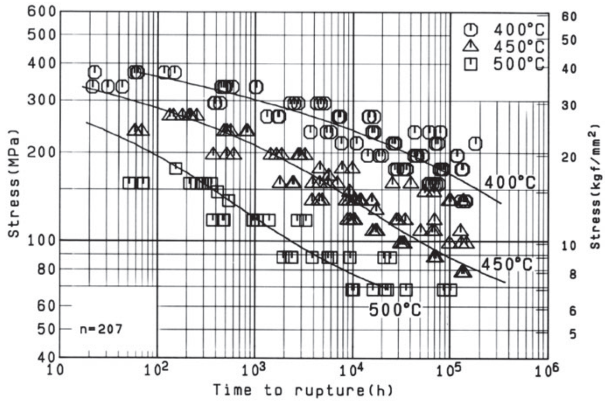

Fig. 17 Creep rupture strength of carbon steel (JIS STB 410).

after long-term creep for both steels together with the formation of PFZ. This indicates that deformation resistance is higher in the grain interior than in the PFZ after long-term creep exposure. The difference in the deformation resistance between the grain interior and the PFZ is higher in KA-SUS304J1HTB than in SUS304HTB because the precipitation strengthening in the grain interior is very high in KA-SUS304J1HTB. This leads to the remarkable drop in creep strength for KA-SUS304J1HTB as compared with SUS304HTB as shown in Fig. 12. For example, the effect of PFZ formation on creep strength can be explained by a "core–mantle" model [66] to explain the grain-size dependence of the creep rate.

4. Heat-to-Heat Variation of Creep Strength

Figure 17 shows the creep rupture strength of carbon steel, JIS STB 410 [27]. The data were obtained from 9 heats that were in the range of the material specification. Three steelmakers supplied the materials for creep testing [27]. The heat-to-heat variation of creep rupture strength is very clear at all testing temperatures even in the range of the material specification. At 400°C, the difference in creep rupture time is one order of magnitude. It is predicted that the SEE value in eq. (6) will be large, indicating that the allowable stress is estimated to be small because of low minimum creep strength. The reason for the large difference in creep rupture time is due to the difference in Mo content [67], although the Mo content is not specified in JIS STB 410 [29]. The relationship between stress and LM parameter of JIS STB 410 is shown in Fig. 18 together with Mo content [67]. The creep strength apparently increases with increasing Mo content even in the range of the material specification. It was reported that an increase in Mo-C atomic pairs can increase the creep strength in carbon steel based on the calculation of the equilibrium solute elements and atomic pairs by Thermo-calc [68]. Therefore, it is possible that an appropriate allowable stress can be established if the Mo content is specified in JIS STB 410.

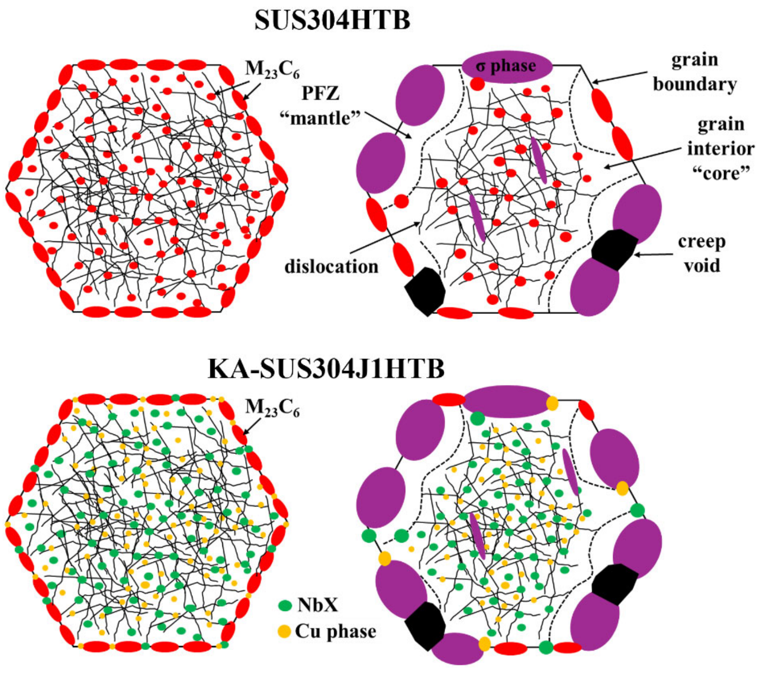

Fig. 16 Schematic illustrations of microstructural changes during creep exposure for SUS304HTB and KA-SUS304J1HTB. Left hand side: after short-term creep, Right hand side: after long-term creep. (online color)

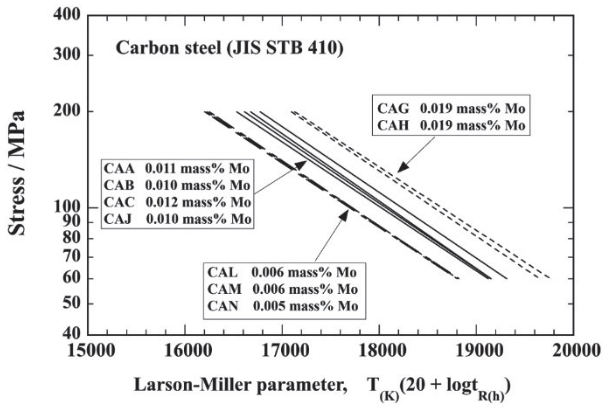

Fig. 18 Relationship between stress and Larson-Miller parameter for carbon steel (JIS STB 410). CAA, CAB, CAC, CAG, CAH, CAJ, CAL, CAM, CAN: heat name.

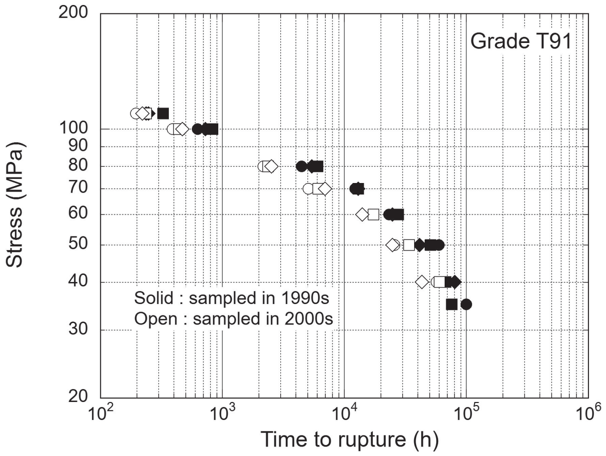

Fig. 19 Creep rupture strength of Grade 91 steels at 650°C.

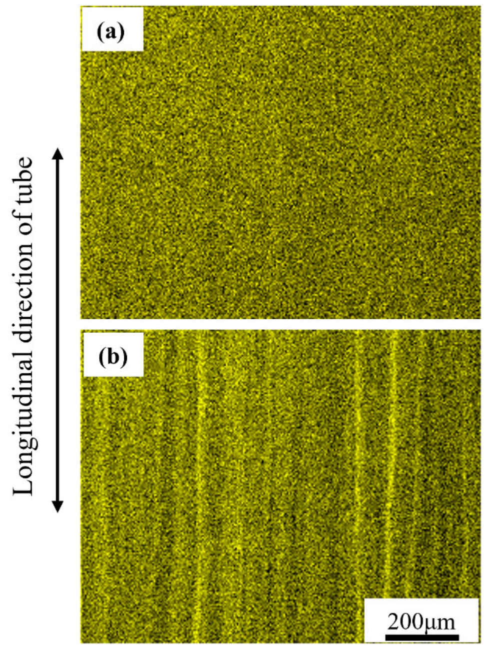

Fig. 20 Results of Cr mapping by SEM-EDS for as received sample after renormalizing in Grade 91. (a) MGB heat, (b) MGG heat. (online color)

Figure 2 shows the creep rupture strength of ASME Grade 91 steel tubes [22] including 6 heats from several steel-makers. The heat-to-heat variation of creep rupture strength is clearly seen at 600°C to 650°C. No correlation between Ni and Al contents and creep rupture strength was confirmed [69] although it was reported that the increase in Ni [70] and Al [71] content decreases the creep rupture strength. The creep rupture strength at 650°C is shown in Fig. 19. It seems that the creep rupture data can be divided into two groups by sampling year. The solid and open symbols mean the heat sampled in the 1990s and 2000s, respectively. However, the sampling year cannot be the reason for the heat-to-heat variation. In addition to the chemical compositions, a difference in initial microstructure can cause a difference in creep rupture strength. Figure 20 shows the results of elemental mapping of Cr after renormalizing for as received samples of ASME Grade 91. The Cr segregates along the longitudinal direction of the boiler tube for MGG heat as compared with MGB heat as shown in Fig. 20. Normally, $M_{23}C_6$ and MX precipitates are formed after normalizing and tempering in the steel. However, $M_{23}C_6$ and MX precipitates can dissolve in the matrix after renormalizing. The Cr segregation shown in Fig. 20 corresponds to Cr from dissolved $M_{23}C_6$ because M in $M_{23}C_6$ is Cr and Mo for Grade 91 steel. MGB and MGG heats were sampled in the 1990s and 2000s, respectively. Therefore, the creep strength is lower in MGG heat than in MGB heat, meaning that the Cr segregation decreases the creep strength [69]. It was reported [69] that the decrease in number of $M_{23}C_6$ precipitates during creep exposure was more remarkable in MGG heat than in MGB heat. Furthermore, recovery of martensitic structure during creep exposure was faster in MGG heat than in MGB heat [69]. The precipitates and martensite structure strengthening significantly decrease during creep exposure in the strongly segregated heat. The difference in these microstructural changes can cause the difference in creep strength between the two heats. The effect of segregation along the longitudinal direction of the boiler tube on creep strength was reported for not only Grade 91 but also Grade 92 steels [72]. Ideally, the effect of chemical composition on the creep strength should be discussed for a material in which segregation is eliminated. Since it may be difficult to eliminate the segregation during the manufacturing process of a commercial steel, it is recommended to specify the reduction of the segregation in the material specification.

For 700°C, the creep rupture strengths of austenitic heat-resistant steels are shown in Fig. 21 [58, 73, 74]. The data are obtained from several heats for each steel. The heat-to-heat variations of creep rupture strength are clearly observed for each steel even for the same material specification. It was reported that a correlation between solute nitrogen content and creep rupture time was observed for SUS304HTB [75]. For SUS321HTB (18Cr-10Ni-Ti), the creep rupture time increased with increasing grain size [75]. The increase in boron content increased the creep rupture time of SUS347HTB (18Cr-12Ni-Nb) even in the range of the material specification [75]. The heat-to-heat variation of creep strength is observed for not only heat-resistant steels but also Ni based alloys such as JIS NCF718-B [76].

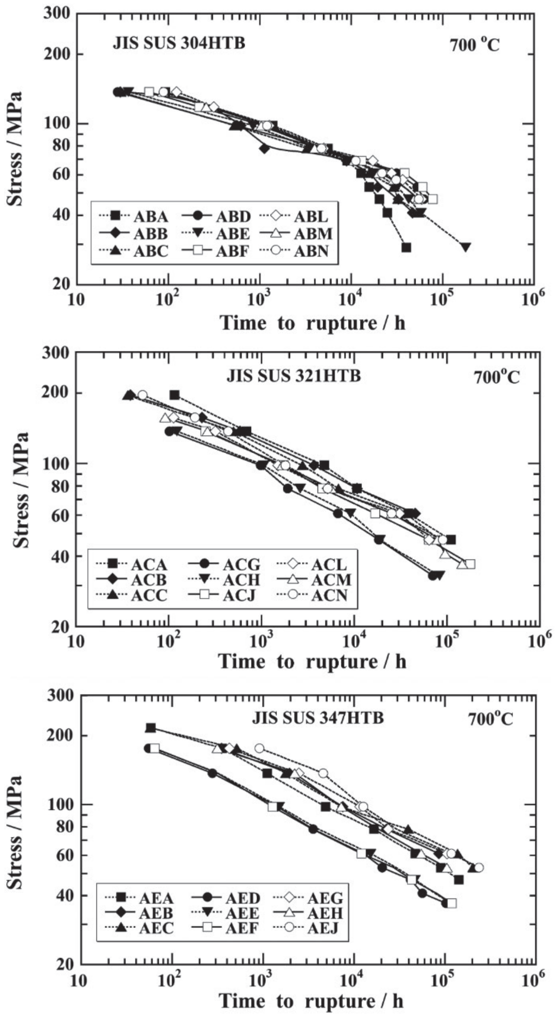

Fig. 21 Creep rupture strengths of SUS304HTB, SUS321HTB and SUS347HTB.

5. Creep Strength Evaluation and Allowable Stress in Future

For a commercial steel it is difficult to avoid creep strength degradation in the long term because the precipitation and dislocation strengthening will decrease during creep exposure as shown in section 3. Furthermore, deformation and fracture mechanisms may change depending on the stress conditions. The methods such as region-splitting analysis and multi-region analysis mentioned in section 2 are suitable for evaluating creep strength when creep strength degradation occurs. Therefore, for a developed material, not only creep rupture data but also information on microstructural changes during creep exposure should be considered to evaluate long-term creep strength and establish an allowable stress. For next-generation nuclear reactors, the 60-year creep rupture strength should be evaluated. In this case, creep rupture data and data of microstructural changes in the very long term will be needed to clarify whether a method such as region-splitting analysis should be applied or not.

In order to establish an allowable stress, the minimum creep strength estimated from eq. (6) is also needed. The minimum creep strength decreases when the heat-to-heat variation of creep strength is large as mentioned in section 2. For developing a new material, in addition to improving average creep strength, it is important to minimize the heat-to-heat variation of creep strength. The range of chemical composition and manufacturing process can affect the heat-to-heat variation of creep strength as mentioned in section 4, indicating that robustness is needed for a new heat-resistant material. Recently, additively manufactured (AM) materials are being developed as heat-resistant materials [26, 77, 78], and these materials are also actively being standardized in the ASME code [79]. For AM materials, printing parameters and build direction may be new factors that affect the heat-to-heat variation of creep strength.

It is easy to predict long-term creep strength when no remarkable microstructural changes occur during creep exposure. Ideally, solid solution strengthened materials without precipitation strengthening are suitable for heat-resistant materials, but these have not yet been achieved.

Acknowledgement

The author thanks Dr. Kazuhiro Kimura, Dr. Tomotaka Hatakeyama, Mr. Yasushi Taniuchi, Dr. Kaoru Sekido, Mr. Takehiro Nojima and other people involved in the NIMS Creep Data Sheet Project.

REFERENCES

[1] S. Zhang and Y. Takahashi: Effect of variable loading on creep property of Mod.9Cr-1Mo steel and life evaluation, Proceedings of the 60th Symposium on Strength of Materials at High Temperatures, (The Society of Materials Science, Kyoto, 2022) pp. 1–5.
[2] F. Abe, T.U. Kern and R. Viswanathan: *Creep-resistant Steels*, (Woodhead Publishing Limited, 2008) pp. 446–471.
[3] D. Osorio, A. Gotti, F. Kauffmann and A. Klenk: Creep, fatigue and creep-fatigue behaviour of martensitic/bainitic steels and nickel-based alloys and their welded joints at the temperature range 500°C–750°C, Mater. High Temp. **41** (2024) 2–30.
[4] Successful Demonstration Test of Ammonia Firing Conducted at Commercial Power Station, IHI Engineering Review **58** (2025) 1–6.
[5] K. Kurita, H. Sakaba, H. Mochida, M. Kawamura and M. Uzawa: Activities for Constructing a Demonstration Fast Reactor as a Core Company, Mitsubishi Heavy Industries Technical Review **61** (2025) 1–7.
[6] H. Onishi, K. Asano, W. Sakuma, S. Oyama, K. Yamaji and T. Hara: Development of High Temperature Gas-cooled Reactor for Hydrogen Production System, Mitsubishi Heavy Industries Technical Review **61** (2025) 1–8.
[7] T. Onizawa, T. Asayama and K. Kikuchi: Development of High Chromium Steel for Fast Breeder Reactors with High-temperature Strength, Ductility, and Microstructural Stability, ISIJ Int. **53** (2013) 1081–1088.
[8] American Society of Mechanical Engineers (ASME), ASME boiler and pressure vessel conde, Section III, Division 5, (2019).
[9] T. Hamaguchi, S. Kurihara, H. Hirata and H. Okada: Creep rupture properties and microstructures of 9Cr–3Co–3W-Nd-B steel welded joints, Mater. Sci. Eng. A **831** (2022) 142231.

[10] H. Semba and H. Okada: Creep Strength and Microstructure of Ni-Base HR6W Tubes & Pipes for High Efficiency Fossil Power Plant, Materia Japan **55** (2016) 453–456.
[11] K. Kimura: Assessment of long-term creep strength and review of allowable stress of high Cr ferritic creep resistant steels, Proceedings of 2005 ASME Pressure Vessels and Piping Division Conference, (ASME) PVP2005-71039.
[12] K. Kimura and M. Yaguchi: Re-evaluation of long-term creep strength of base metal of Grade 91 type steel, Proceedings of the ASME 2016 Pressure Vessels and Piping Conference, (ASME) PVP2016-63355.
[13] H. Kushima, K. Kimura and F. Abe: Degradation of Mod.9Cr-1Mo steel during long-term creep deformation, Tetsu-to-Hagané **85** (1999) 841–847.
[14] K. Kimura, H. Kushima and F. Abe: Improvement of creep life prediction of high Cr ferritic creep resistant steels by region partitioning method of stress vs. time to rupture diagram, J. Soc. Mat. Sci., Japan **52** (2003) 57–62.
[15] F.R. Larson and J. Miller: A Time-Temperature Relationship for Rupture and Creep Stresses, Trans. ASME **74** (1952) 765–771.
[16] American Society of Mechanical Engineers (ASME), ASME boiler and pressure vessel conde, Section II, Part D, (2023).
[17] K. Sawada, Y. Taniuchi, K. Sekido, T. Nojima and K. Kimura: Evaluation of 100,000 h creep rupture strength of low alloy steels, Tetsu-to-Hagané **108** (2022) 679–685.
[18] K. Sawada, K. Kimura, F. Abe, Y. Taniuchi, K. Sekido, T. Nojima, T. Ohba, H. Kushima, H. Miyazaki, H. Hongo and T. Watanabe: Catalog of NIMS creep data sheets, Sci. Technol. Adv. Mater. **20** (2019) 1131–1149.
[19] R.L. Orr, O.D. Sherby and J.E. Dorn: Correlations of Rupture Data for Metals at Elevated Temperatures, Trans. ASM **46** (1954) 113–118.
[20] S.S. Manson and A. Haferd: A linear time-temperature relation for extrapolation of creep and stress rupture data, National Advisory Committee for Aeronautics 1953 (TN2890).
[21] K. Kimura: Creep Rupture Life Prediction of Creep Resistant Steels, J. Japan Inst. Metals **73** (2009) 323–333.
[22] K. Kimura, Y. Taniuchi, K. Sekido, T. Nojima, T. Hatakeyama and K. Sawada: Creep data sheet for 9Cr-1Mo-V-Nb steel tubes, plates and pipe, Sci. Tech. Adv. Mater.: Methods **5** (2025) 2588872.
[23] K. Maruyama, H.G. Armaki, R.P. Chen, K. Yoshimi, M. Yoshizawa and M. Igarashi: Cr concentration dependence of overestimation of long term creep life in strength enhanced high Cr ferritic steels, Int. J. Press. Vessels Piping **87** (2010) 276–281.
[24] K. Maruyama, J. Nakamura and K. Yoshimi: Assessment of Long-Term Creep Rupture Strength of T91 Steel by Multiregion Rupture Data Analysis, J. Press. Vess. Technol. **138** (2016) 031407.
[25] K. Sawada, T. Hatakeyama, M. Kusano and M. Watanabe: Creep data of Hastelloy X fabricated by laser powder bed fusion, Sci. Tech. Adv. Mater.: Methods **5** (2025) 2582996.
[26] T. Hatakeyama, K. Sawada, M. Kusano and M. Watanabe: Significant creep-strength improvement in modified 9Cr-1Mo steel via micro-structural control through laser powder bed fusion, Addit. Manuf. **93** (2024) 104445.
[27] NRIM Creep Data Sheet No. 7B (National Research Institute for Metals, 1992).
[28] NIMS Creep Data Sheet No. M-13 (National Institute for Materials Science, 2021).
[29] S. Yokoi, N. Shinya, M. Kori and H. Tanaka: Some causes of scattering in rupture strength Silicon-Killed carbon steel for boiler tube, J. Soc. Mat. Sci., Japan **25** (1976) 249–255.
[30] T. Hatakeyama, K. Sawada, K. Sekido, T. Hara and K. Kimura: Graphitization Behaviors of Creep-ruptured 0.3% Carbon Steel at 673 to 773 K, ISIJ Int. **61** (2021) 993–1001.
[31] JIS B 8265: 2017, Construction of pressure vessel - General principles.
[32] JPI-8S-1-2018: 2018, Piping inspection and maintenance.
[33] H.C. Furtado and I. Le May: Evaluation of an unusual superheated steam pipe failure, Mater. Charact. **49** (2002) 431–436.
[34] T. Hatakeyama, K. Sawada, K. Sekido, T. Hara and K. Kimura: TTP Diagrams of Graphitization of Creep Ruptured Carbon Steels and 0.5Mo Steel, ISIJ Int. **61** (2021) 2822–2831.
[35] NIMS Creep Data Sheet No. M-4 (National Institute for Materials Science, 2005).
[36] K. Kimura, H. Kushima, E. Baba, T. Shimizu, Y. Asai, F. Abe and K. Yagi: Effect of initial microstructure on long term creep strength of a low alloy ferritic steel, Tetsu-to-Hagané **86** (2000) 542–549.
[37] T.D. Nguyen, K. Sawada, H. Kushima, M. Tabuchi and K. Kimura: Change of precipitate free zone during long-term creep in 2.25Cr–1Mo steel, Mater. Sci. Eng. A **591** (2014) 130–135.
[38] F. Masuyama: History of Power Plants and Progress in Heat Resistant Steels, ISIJ Int. **41** (2001) 612–625.
[39] American Society of Mechanical Engineers (ASME), ASME boiler and pressure vessel conde, Section II, Part A, (2019).
[40] K. Maruyama, K. Sawada and J. Koike: Strengthening Mechanisms of Creep Resistant Tempered Martensitic Steel, ISIJ Int. **41** (2001) 641–653.
[41] Y. Kadoya and E. Shimizu: Effect of Solute Mo and W on Transient Creep Deformation of High-Cr Ferritic Steels, Tetsu-to-Hagané **86** (2000) 617–624.
[42] K. Sawada, H. Kushima, M. Tabuchi and K. Kimura: Microstructural degradation of Gr.91 steel during creep under low stress, Mater. Sci. Eng. A **528** (2011) 5511–5518.
[43] K. Sawada, K. Sekido, H. Kushima and K. Kimura: Microstructural degradation during long-term creep in 9–12%Cr steels, Proc. of 4th ECCC Creep & Fracture Conference, (The European Creep Collaborative Committee, 2017) No. 96 (USB).
[44] F. Abe: Coarsening Behavior of Martensite Laths in Tempered Martensitic 9Cr-W Steels during Creep Deformation, Proc. the fourth Inter. Conf. Recrystallization and Related Phenomena, (The Japan Institute of Metals, 1999) pp. 289–294.
[45] Y. Kadoya, B.F. Dyson and M. McLean: Microstructural Stability during Creep of Mo- or W-Bearing 12Cr Steels, Metall. Mater. Trans. A **33** (2002) 2549–2557.
[46] T. Horiuchi, M. Igarashi and F. Abe: Improved Utilization of Added B in 9Cr Heat-Resistant Steels Containing W, ISIJ Int. **42** (2002) S67–S71.
[47] T. Okano, T. Ito, M. Mitsuhara and M. Nishida: Effect of grain boundary characters on $M_{23}C_6$ coarsening in 9Cr ferritic heat-resistant steel, CAMP-ISIJ **29** (2016) 319.
[48] H.K. Danielsen and J. Hald: Behaviour of Z phase in 9–12%Cr steels, Energy Mater. **1** (2006) 49–57.
[49] L. Cipolla, H.K. Danielsen, D. Venditti, P.E. Di Nunzioa, J. Hald and M.A.J. Somers: Conversion of MX nitrides to Z-phase in a martensitic 12% Cr steel, Acta Mater. **58** (2010) 669–679.
[50] K. Sawada, H. Kushima, K. Kimura and M. Tabuchi: TTP Diagrams of Z Phase in 9–12% Cr Heat-Resistant Steels, ISIJ Int. **47** (2007) 733–739.
[51] A. Strang and V. Vodarek: Microstructural degradation of martensitic 12%Cr power plant steels during prolonged high temperature creep exposure, Proc. of Materials for Advanced Power Engineering, (Forschungszentrum Julich GmbH, 1998) pp. 603–614.
[52] K. Sawada, H. Kushima, T. Hara, M. Tabuchi and K. Kimura: Heat-to-heat variation of creep strength and long-term stability of micro-structure in Grade 91 steels, Mater. Sci. Eng. A **597** (2014) 164–170.
[53] H.K. Danielsen and J. Hald: A thermodynamic model of the Z-phase Cr(V, Nb)N, Calphad **31** (2007) 505–514.
[54] C.R. Brinkman, B. Gieseke and P.J. Maziasz: The influence of long thermal aging on the microstructure and mechanical properties of modified 9Cr-1Mo steel, Proc. Microstructure and Mechanical Properties of Aging Materials, (The Minerals, Metals & Materials Society, 1993) pp. 107–115.
[55] J. Hald and L. Korcakova: Precipitate Stability in Creep Resistant Ferritic Steels Experimental Investigations and Modelling, ISIJ Int. **43** (2003) 420–427.
[56] J.S. Lee, H.G. Armaki, K. Maruyama, T. Muraki and H. Asahi: Causes of breakdown of creep strength in 9Cr–1.8W–0.5Mo–VNb steel, Mater. Sci. Eng. A **428** (2006) 270–275.
[57] NIMS Creep Data Sheet No. 56A (National Institute for Materials Science, 2018).
[58] NRIM Creep Data Sheet No. 4B (National Research Institute for Metals, 1986).
[59] Y. Sawaragi, K. Ogawa, S. Kato, A. Natori and S. Hirano: Development of the economical 18-8 stainless steel (Super 304H) having high elevated temperature strength for fossil fired boilers, Sumitomo Search **48** (1992) 50–58.
[60] T. Hatakeyama, K. Sawada, K. Sekido, T. Hara and K. Kimura: Mater.

Sci. Eng. A **831** (2022) 142225.
[61] K. Sawada, K. Sekido, M. Murata, K. Kamihira and K. Kimura: Precipitation behavior during aging and creep in 18Cr–9Ni–3Cu–Nb–N steel, Mater. Charact. **141** (2018) 279–285.
[62] S. Kobayashi, M. Murata, K. Kamihira and K. Kimura: The degradation of long-term creep strength and microstructure evolution in SUPER304H, Proc. Creep and Fracture in High-Temperature Components: Design and Life Assessment, (INAIL, 2014) pp. 760–765.
[63] NRIM Creep Data Sheet No. M-1 (National Research Institute for Metals, 1999).
[64] NIMS Creep Data Sheet No. M-11 (National Institute for Materials Science, 2016).
[65] K. Sawada, T. Hatakeyama, K. Sekido and K. Kimura: Microstructural changes and creep-strength degradation in 18Cr-9Ni-3Cu-Nb-N steel, Mater. Charact. **178** (2021) 111286.
[66] Y. Terada, T. Matsuo and M. Kikuchi: Effect of grain boundaries on creep deformation in austenitic alloys, Proc. of Aspects of High Temperature Deformation and Fracture, (The Japan Inst. Met. Mater., 1993) pp. 27–34.
[67] K. Kimura, H. Kushima, K. Yagi and C. Tanaka: Effects of Minor Alloying Elements on Inherent Creep Strength Properties of Ferritic Steels, Trans. Iron Steel Inst. Jpn. **81** (1995) 757–762.
[68] H. Onodera, T. Abe, M. Ohnuma, K. Kimura, M. Fujita and C. Tanaka: Effect of Minute Solute Elements in the Ferrite Matrix on the Inherent Creep Strength of Carbon Steels, Trans. Iron Steel Inst. Jpn. **81** (1995) 821–826.
[69] K. Sawada, K. Sekido, K. Kimura, K. Arisue, M. Honda, N. Komai, N. Fukuzawa, T. Ueno, N. Shimohata, H. Nakatomi, K. Takagi, T. Kimura, K. Nomura and K. Kubushiro: Effect of Initial Microstructure on Creep Strength of ASME Grade T91 Steel, ISIJ Int. **60** (2020) 382–391.
[70] K. Kimura, K. Sawada, H. Kushima and Y. Toda: Influence of Chemical Composition and Heat Treatment on Long-term Creep Strength of Grade 91 Steel, Procedia Eng. **55** (2013) 2–9.
[71] N. Komai, K. Arisue, N. Saito, K. Tominaga and M. Fujita: Effect of chemical composition on the creep rupture strength of Mod.9Cr-1Mo steel weldments, Proc. 1st Inter. Conf. Advanced High-Temperature Materials Technology for Sustainable and Reliable Power Engineering, (The 123rd Committee of Japan Society for the Promotion of Science, IAI., 2015) pp. 57–60.
[72] K. Sawada, K. Sekido and K. Kimura: Segregation and its effect on creep rupture strength in Grade 92 steels, Mater. Charact. **169** (2020) 110581.
[73] NRIM Creep Data Sheet No. 5B (National Research Institute for Metals, 1987).
[74] NRIM Creep Data Sheet No. 28B (National Research Institute for Metals, 2001).
[75] F. Abe: Heat-to-Heat Variation in Creep Life and Fundamental Creep Rupture Strength of 18Cr–8Ni, 18Cr–12Ni–Mo, 18Cr–10Ni–Ti, and 18Cr–12Ni–Nb Stainless Steels, Metall. Mater. Trans. A **47** (2016) 4437–4454.
[76] K. Sawada, Y. Taniuchi, K. Sekido, T. Nojima, T. Hatakeyama and K. Kimura: Creep data sheet for Nickel-based 19Cr-18Fe-3Mo-5Nb-Ti-Al superalloy, Sci. Tech. Adv. Mater.: Methods **4** (2024) 2425179.
[77] B. Sutton, E. Jang, S. Tate and J. Shingledecker: Assessment of 316H Stainless Steel Produced by Directed Energy Deposition Additive Manufacturing for High Temperature Power Plant Applications, Proc. Advances in Materials, Manufacturing, and Repair for Power Plants, (ASM International, 2024) pp. 1020–1032.
[78] O. El-Atwani, B.P. Eftink, C.M. Cady, D.R. Coughlin, M.M. Schneider and S.A. Maloy: Enhanced mechanical properties of additive manufactured Grade 91 steel, Scr. Mater. **199** (2021) 113888.
[79] Argonne National Lab., Anl-ammt-009, ASME code qualification plan for LPBF 316, SS, (2023).